Precise analysis of the timing performance of Cherenkov-radiator-integrated MCP-PMTs: analytical deconvolution of MCP direct interactions

Physics in Medicine & Biology

NOTE

Precise analysis of the timing performance of Cherenkov-radiator-integrated MCP-PMTs: analytical deconvolution of MCP direct interactions

IOP Publishing Phys. Med. Biol. 65 (2020) 10NT03 https://doi.org/10.1088/1361-6560/ab8c8f

Physics in Medicine & Biology

IPEM Institute of Physics and Engineering in Medicine

CrossMark

RECEIVED
23 December 2019

REVISED
2 April 2020

ACCEPTED FOR PUBLICATION
23 April 2020

PUBLISHED
29 May 2020

NOTE

Precise analysis of the timing performance of Cherenkov-radiator-integrated MCP-PMTs: analytical deconvolution of MCP direct interactions

R Ota[1,2], **K Nakajima**[2], **I Ogawa**[2], **Y Tamagawa**[2], **H Shimoi**[3], **M Suyama**[4] **and T Hasegawa**[5]

[1] Central Research Laboratory, Hamamatsu Photonics K. K., Hamamatsu, Japan
[2] Graduate School of Engineering, University of Fukui, Fukui, Japan
[3] Electron Tube Division, Hamamatsu Photonics K. K., Hamamatsu, Japan
[4] Global Strategic Challenge Center, Hamamatsu Photonics K. K., Hamamatsu, Japan
[5] School of Allied Health Science, Kitasato University, Kitasato, Japan

E-mail: ryosuke.ota@crl.hpk.co.jp

Keywords: micro channel plate photomultiplier tube (MCP-PMT), MCP direct interaction, coincidence time resolution (CTR)

Abstract

In order to achieve the ultimate goal of reducing coincidence time resolution (CTR) to 10 ps, thus enabling reconstruction-less positron emission tomography, a Cherenkov-radiator-integrated microchannel plate photomultiplier tube (CRI) reaching CTR of sub-50 ps full width at half maximum (FWHM) has been developed. However, a histogram of time differences between a pair of the CRIs shows undesirable side peaks, which are caused by gamma rays directly interacting with the micro channel plates (MCPs). Such direct interaction events are detrimental to the timing performance of the CRI. In this paper, we demonstrate an analytical method of deconvolving MCP direct interaction events from the timing histogram. Considering the information of the main and the two side peaks, the timing uncertainty caused by the MCP direct interaction events is deconvolved and the CTR of the CRI is analytically investigated. Consequently, the CTR is improved from 41.7 to 40.5 ps FWHM by the deconvolution. It means that a mixture of the Cherenkov radiator events and the MCP direct interaction events contribute to the CTR by a factor of 10 ps. The timing performance of the MCP direct interaction events are also evaluated. The CTR between the two MCPs is found to be 66.2 ps FWHM. This indicates that a photocathode-free radiation detector with high timing performance is possible. Elimination of the photocathode from the detector would make detector construction easier and more robust.

1. Introduction

Due to recent drastic improvement of both photodetectors and luminescent materials, the coincidence time resolution (CTR) of detectors dedicated to time-of-flight positron emission tomography (TOF-PET) has been improved. Currently, several TOF-PET scanners are commercially available, and their system CTRs range from 200 to 600 ps (Vandenberghe *et al* 2016, Hsu *et al* 2017, Rausch *et al* 2019, Sluis *et al* 2019). Because a CTR of 200 ps is equivalent to a position resolution of 30 mm along the line of response (LOR) of the pair of PET detectors, the signal to noise ratio of the PET image can be successfully improved compared to non TOF-PET (Conti 2009). However, as the position resolution of 30 mm is larger than the spatial (x,y) resolution of clinical PET scanners, image reconstruction processes are still required. If the CTR ultimately reached 10 ps, the position resolution along the LOR would reach 1.5 mm. In that case, the image reconstruction processes, which tend to amplify the noise of the PET images, would not be necessary because the TOF information can directly provide the position of annihilation positrons (Gundacker *et al* 2016, Lecoq 2017, Ota *et al* 2019a). As the spatial resolution of the current clinical TOF-PET scanners is 3–5 mm, the constraints on the CTR can be relaxed to 20–35 ps FWHM (Gundacker *et al* 2016). To achieve this ambitious goal, the entire detection chain, from gamma-ray interaction with the materials to the readout electronics should be fully understood.

As a physical phenomenon, Cherenkov radiation has been received attention due to its prompt emission, thus enhancing the CTR (Lecoq *et al* 2010, 2014). Even a Thallium bromide (TlBr) detector, which is a semiconductor detector, can reach a CTR of 300–400 ps FWHM with high energy resolution by extracting and using the Cherenkov photons yielded by the TlBr crystal (Arino-Estrada *et al* 2018, 2019), whereas its CTR without Cherenkov photons has reported as nano-second order (Hitomi *et al* 2013).

Moreover, Cherenkov photons can push the limits of the CTR of scintillation detectors regardless of the speed of the scintillators (Kwon *et al*, 2016, Gundacker *et al*, 2016, Brunner and Schaart 2017, Cates and Levin 2019). Bismuth germanate (BGO) scintillators are cheap and have high stopping power, but the material is not suitable for TOF-PET applications due to its relatively slow decay time (60 and 300 ns, Moszynski *et al* 1981). By detecting the Cherenkov photons using a silicon photomultiplier (SiPM) with high photo detection efficiency (PDE), however, BGO shows potential as a scintillator for TOF-PET. The CTR of detectors made from a small BGO crystal and the SiPM approaches or exceeds 200 ps FWHM. However, in the case of the BGO detector, timing histograms are more likely to fit a Lorentz function rather than Gaussian. This means that the histogram has longer full width at tenth maximum (FWTM). The Lorentzian shape occurs because the timing histogram is a mixture of signals caused by both fast Cherenkov and slow scintillation photons. The long FWTM inhibits the benefits of the short FWHM (Kwon *et al*).

As the Cherenkov photons are promptly emitted before scintillation photons are emitted, triggering the first photon is important to effectively select the Cherenkov photon (Gundacker *et al*). Using high-frequency-electronics for SiPM readout (Cates *et al* 2018) is one technique used to detect the first photon because it allows for lowering the leading-edge threshold level to approach the electronic noise level. However, signals derived from the scintillation photons could not be eliminated from the timing histogram due to the finite PDE of the SiPM. The finite PDE of the SiPM implies that the Cherenkov photons do not always provide the timing information, whereas the scintillation photons sometimes do. Regarding the scintillation properties of the BGO, such as light yield, and rise and decay times, the timing uncertainty triggered by the scintillation photons is relatively worse than that triggered by the Cherenkov photons. Thus, the signals derived from the scintillation photons worsen timing performance.

A pure Cherenkov radiator, such as a lead glass or lead fluoride, does not produce the long tail triggered by scintillation photons because the radiator emits only Cherenkov photons. Timing histograms from a pair of detectors composed of pure Cherenkov radiators and micro channel plate photomultiplier tubes (MCP-PMT) form a Gaussian shape (Ota *et al* 2019a, 2019b). The CTR of the Cherenkov detector is highly affected by the single photon time resolution (SPTR) of the photodetector (Ota *et al* 2018). Thanks to the good SPTR of the MCP-PMT (25 ps FWHM), CTRs of sub-50 ps FWHM has been achieved. However, the gamma rays interact with MCP, which causes another sharp peak on the timing histogram (Ota *et al* 2019a, 2019b). In fact, the MCP itself can function as a direct gamma-ray detector with high timing performance of 20–30 ps σ according to previous reports (Barnyakov *et al* 2017, 2018). In the case where two gamma rays interact with the radiators or with the MCPs, the interactions cannot be separated from the waveform information. Although the timing performance of the MCP direct event is high, a mixture of radiator events and MCP events would deteriorate the overall timing performance of the detector pair. Therefore, those types of interactions should be separated.

In this paper, we report an analytical method for deconvolving the MCP direct events from a histogram of time differences experimentally obtained using a pair of Cherenkov-radiator-integrated (CRI) MCP-PMTs (Ota *et al* 2019a) and show the precise timing performance of the CRI. In addition, we demonstrate how the MCP direct interaction affects the timing performance of the CRI.

2. Materials and methods

2.1. Cherenkov-radiator-integrated MCP-PMT (CRI) and experimental setup

The CRI has an active area of 11 mmϕ $\times$ 3.2 mm lead glass radiator, and an overall length and outer diameter of 70.2 mm and 45.0 mm, respectively. An Al_2O_3 layer is inserted between the photocathode and the lead glass using the atomic layer deposition (ALD) technique to suppress chemical reaction between the photocathode and the lead glass. Owing to the advantages of the ALD technique, the thickness of the Al_2O_3 layer is only a few nanometers, which is relatively lesser than the wavelength of the Cherenkov photons. Therefore, approximately no optical boundaries exist from the radiator to the photocathode. Note that both the MCP and the Cherenkov radiator are composed of lead glass; they mainly consist of PbO and SiO_2, and has a density of 3.93 g cm^{-3}. The total attenuation length of this lead glass is approximately 22.4 mm (National Institute of Standards and Technology). Thus, as described in the introduction section, the gamma rays can directly interact with the MCP because of its large effective atomic number.

The experimental setup is identical to Ota *et al* (2019a) except for the distance between the CRIs, which is 200 mm. The entrance surface of the lead glass was covered by a black tape (Super 33+, 3M) to suppress reflections of the Cherenkov photons in the lead glass radiator. A high voltage of −3100 V was supplied to each CRI, where the gain is approximately 5.0×10^5. A ^{22}Na point source was placed at the center of the CRIs with a 50 mm thick lead collimator. The waveforms are fully digitized by an oscilloscope with a set bandwidth of 4.2 GHz and a sampling rate of 20 GS s^{-1} (50 ps time bin) only when both CRIs detect gamma rays in coincidence. The digitized data was analyzed using ROOT software (Brun and Rademakers 1997). First, spline curves are obtained from the digitized waveforms using the TSpline3 class method implemented in ROOT. Then, the baseline, pulse height, and detection timing, which are numerically calculated using the spline curve at arbitrary timing pick-off threshold levels, are calculated. In this study, the timing pick-off threshold level was defined as the ratio of the pulse height to perform the time walk correction completely. The timing pick-off threshold level was set to 5% for pulse height, which optimizes the timing performance. Event cuts based on the pulse height or pulse area were not conducted in this study.

2.2. Timing histogram of a pair of CRIs

Timing histograms obtained from the pair of CRIs can be decomposed into several components. The timing histogram, obtained from the experimental setup illustrated in figure 1(a), clearly shows three sharp peaks as depicted in figure 1(b). The t_{right} and t_{left} on the x-axis of figure 1(b) represent the detection timing of the right and the left CRI, respectively. The main center peak includes events where both annihilation gamma rays interacted with each radiator (Radiator–Radiator event) and with each MCP (MCP–MCP event). The side peak includes the events where the two gamma-ray interacted individually with the radiator and the MCP, respectively, and vice versa (Radiator–MCP event or MCP–Radiator event). This interpretation of the histogram can be understood from Ota *et al* (2019b). Additionally, a broad Gaussian distribution on the accidental coincidence events can be seen. The distribution is caused by events where photoelectrons are scattered backward at the MCP surface (Korpar *et al* 2008, Li *et al* 2018). The transit time of the backscattered photoelectron is broadened, resulting in the broad Gaussian distribution.

Consequently, the timing histogram can be divided into six components of (1) Radiator–Radiator, (2) MCP–MCP, (3) Radiator–MCP, (4) MCP–Radiator, (5) Photo-electron backscatter, and (6) accidental coincidence. As can be seen in figure 1(b), other than the Radiator–Radiator and the MCP–MCP events, the peaks can be clearly broken down.

2.3. Analysis for MCP direct interaction

In this section, we describe the analysis method we developed to comprehensively deconvolve the timing uncertainty of the MCP direct interaction and estimate the precise timing performance of the CRIs. This section consists of three parts: (1) relative detection efficiency of the MCP direct interaction is estimated using information from the main and two side peaks, (2) the main peak is resolved into two components of Radiator–Radiator and MCP–MCP events, (3) the timing resolution of the Radiator–Radiator and MCP–MCP events are determined, respectively.

2.3.1. Detection efficiency.

At first, a function of '4 Gaussians + a constant' as described below is fit to the timing histogram of figure 1(b).

$$f(\mathrm{x}) = A_{\mathrm{main}} \exp\left(-\frac{(x-\mu_{\mathrm{main}})^2}{2\sigma_{\mathrm{main}}^2}\right) + A_{\mathrm{left}} \exp\left(-\frac{(x-\mu_{\mathrm{left}})^2}{2\sigma_{\mathrm{left}}^2}\right) + A_{\mathrm{right}} \exp\left(-\frac{(x-\mu_{\mathrm{right}})^2}{2\sigma_{\mathrm{right}}^2}\right) + A_{\mathrm{back}} \exp\left(-\frac{(x-\mu_{\mathrm{back}})^2}{2\sigma_{\mathrm{back}}^2}\right) + C, \quad (1)$$

where A_i, μ_i, σ_i ($i = \mathrm{main, left, right, back}$), and C are the fitting parameters. The fitting region is from −1.25 to +1.25 ns. The parameter C represents the accidental coincidence events. After fitting, all Gaussian areas ($\propto A_i \times \sigma_i$) are calculated and considered physical quantities that are proportional to the detection efficiency. Note that the Gaussian of the main peak contains both Radiator–Radiator and MCP–MCP coincidence events. When the single detection efficiency of the radiator and the MCP are represented by $\varepsilon_{\mathrm{rad}}$ and $\varepsilon_{\mathrm{MCP}}$, respectively, the following relation can be obtained:

$$A_{\mathrm{main}} \times \sigma_{\mathrm{main}} \propto \varepsilon_{\mathrm{rad}}^2 + \varepsilon_{\mathrm{MCP}}^2, \quad (2)$$

$$\frac{(A_{\mathrm{left}} \times \sigma_{\mathrm{left}} + A_{\mathrm{right}} \times \sigma_{\mathrm{right}})}{2} \propto \varepsilon_{\mathrm{rad}} \times \varepsilon_{\mathrm{MCP}}. \quad (3)$$

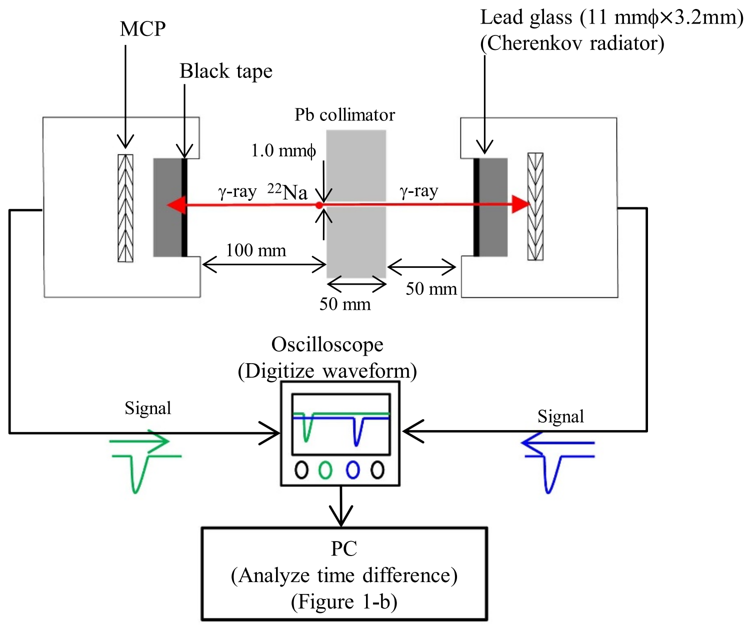

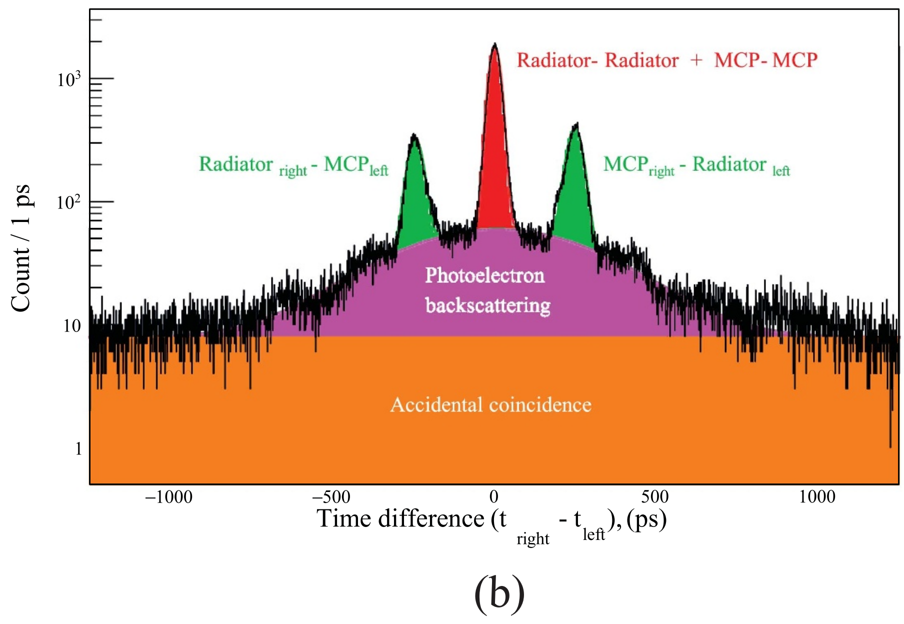

Figure 1. (a) Experimental setup for the measurement of a timing histogram of a pair of CRIs. All parameters except for the distance between the CRIs are the same as Ota *et al* (2019a). (b) Timing histogram obtained from experimental setup shown in (a). The histogram consists of six types of interactions. The main center peak appears to be a single Gaussian, but it contains the two types of interactions.

Here, we hypothesized that the $\varepsilon_{\mathrm{rad}}$ of the right and left detectors are the same and the $\varepsilon_{\mathrm{MCP}}$ of the right and left detectors are the same as well. Both $\varepsilon_{\mathrm{rad}}$ and $\varepsilon_{\mathrm{MCP}}$ can be calculated by solving the simultaneous equations as follows:

$$\frac{\varepsilon_{\mathrm{MCP}}}{\varepsilon_{\mathrm{rad}}} = \frac{A_{\mathrm{left}}\sigma_{\mathrm{left}} + A_{\mathrm{right}}\sigma_{\mathrm{right}}}{A_{\mathrm{main}}\sigma_{\mathrm{main}} + \sqrt{(A_{\mathrm{main}}\sigma_{\mathrm{main}})^2 - (A_{\mathrm{left}}\sigma_{\mathrm{left}} + A_{\mathrm{right}}\sigma_{\mathrm{right}})^2}}. \tag{4}$$

Here, we hypothesized that $\varepsilon_{\mathrm{rad}} < \varepsilon_{\mathrm{MCP}}$. Once $\varepsilon_{\mathrm{MCP}}/\varepsilon_{\mathrm{rad}}$ is obtained, the ratio of Radiator–Radiator and MCP–MCP events in the main peak can also be estimated as $(\varepsilon_{\mathrm{MCP}}/\varepsilon_{\mathrm{rad}})^2$.

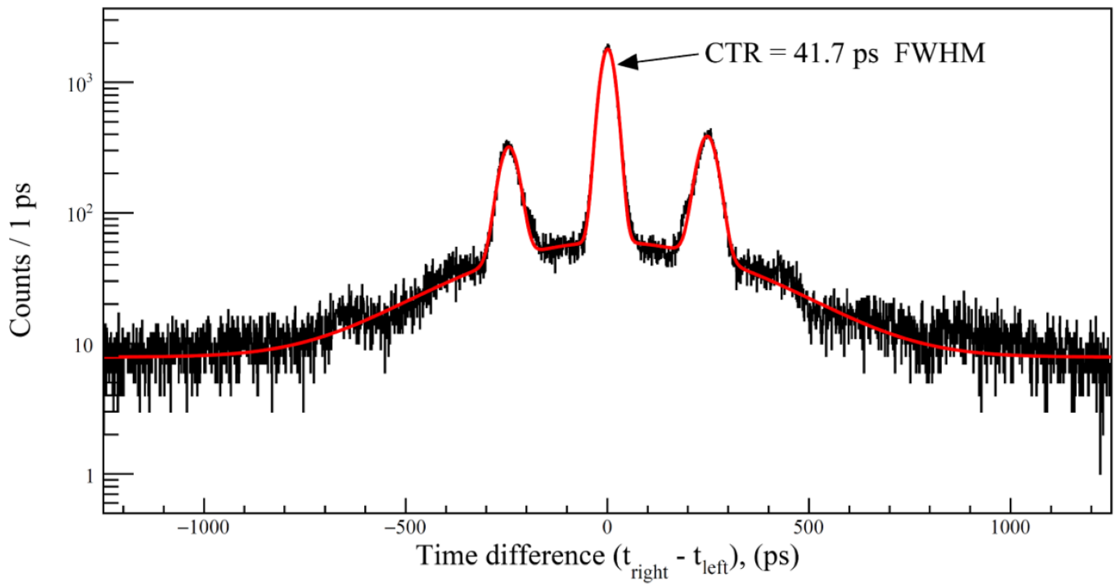

Figure 2. Fitting result of the equation (1) showing an accurate fit to the timing histogram. χ^2/NDF was 1.5. The CTR of the main peak was 41.7 ps FWHM.

2.3.2. Time resolution.

To break down the main peak into its two components, Radiator–Radiator and MCP–MCP events, a function of '3 Gaussians + a constant' is fitted around the main peak (-0.1 ns $< t_{right} - t_{left} < 0.1$ ns):

$$g(x) = A_{rad} \exp\left(-\frac{(x-\mu)^2}{2\sigma_{rad}^2}\right) + A_{rad}\left(\frac{\varepsilon_{MCP}}{\varepsilon_{rad}}\right)^2 \frac{\sigma_{rad}}{\sigma_{MCP}} \exp\left(-\frac{(x-\mu)^2}{2\sigma_{MCP}^2}\right) + A_{back} \exp\left(-\frac{(x-\mu_{back})^2}{2\sigma_{back}^2}\right) + C, \tag{5}$$

$$\sigma_{MCP} = \sqrt{2 \times \left(\left(\frac{\sigma_{right}+\sigma_{left}}{2}\right)^2 - \left(\frac{\sigma_{rad}}{\sqrt{2}}\right)^2\right)}, \tag{6}$$

where A_{rad}, μ, and σ_{rad} are the fitting parameters, and the other parameters A_{back}, μ_{back}, σ_{back}, and C were obtained from equation (1). A factor of $(\sigma_{rad}/\sigma_{MCP})$ in the second term of the right side in the equation (5) is used so that the ratio of the two Gaussian areas is equal to $(\varepsilon_{MCP}/\varepsilon_{rad})^2$. Both parameters σ_{rad} and σ_{MCP} are not considered independent because σ_{MCP} can be calculated once σ_{rad} is obtained. Note that we hypothesized that the mean time μ of the Radiator–Radiator and the MCP–MCP events is the same.

Thus, the CTRs of the Radiator–Radiator and MCP–MCP events can be calculated as σ_{rad} and σ_{MCP} (or in terms of FWHM, as $2.355 \times \sigma$).

3. Results

The fit using equation (1) represented the timing histogram well, as shown in figure 2. χ^2/NDF was 1.5 (=3846/2487). The fit parameters are listed in table 1. From the calculated parameters, $(\varepsilon_{MCP}/\varepsilon_{rad})^2 = 0.062 \pm 0.005$ was obtained. Despite of the thinness of the MCP (0.24 × 2 mm), the detection efficiency of the MCP–MCP events seems to be relatively high. The CTR of the main peak was found to be 17.7 ± 0.1 ps σ (41.7 ± 0.2 ps FWHM).

The fit using equation (5) also matched the timing histogram around the main peak. From the fitting result of the equation (5), the CTR of the Radiator–Radiator and the MCP–MCP events (σ_{rad} and σ_{MCP}) are estimated to be 17.2 ± 0.1 and 28.1 ± 0.3 ps σ (40.5 ± 0.1 and 66.2 ± 0.7 ps FWHM). χ^2/NDF was 1.8 (=361/198). As a result, decomposition of the main peak into two types of events successfully improved the CTR of the Radiator–Radiator event from 41.7 to 40.5 ps. The CTRs of all components are depicted in figure 3.

Relative detection efficiency of the photoelectron backscattering to the Radiator–Radiator events was approximately 50% ($=(A_{back}\sigma_{back})/(A_{main}\sigma_{main}) \times 100$). Because the main peak is approximately composed of only Radiator–Radiator coincidence events, the probability of detecting photoelectrons without backscattering on the surface of the MCP is roughly 80%.

Table 1. Fitting parameters of '4 Gaussians + a constant'. From these parameters, the relative detection efficiency between the radiator and the MCP can be calculated. The relative detection efficiency of $(\varepsilon_{\mathrm{MCP}}/\varepsilon_{\mathrm{rad}})^2 \times 100$ was obtained as 6.2%. The event ratio described on the extreme right is defined as the ratio of a single Gaussian area to the four Gaussian areas.

	A (count ps^{-1})	μ (ps)	σ (ps)	Event ratio (%)
Main peak	1737	1.06	17.7	50.7
Side peak (left)	275	−244	22.8	10.3
Side peak (right)	340	248	23.8	13.4
Photo-electron backscatter	51.6	9.03	306	25.6
Accidental coincidence	7.9	—	—	—

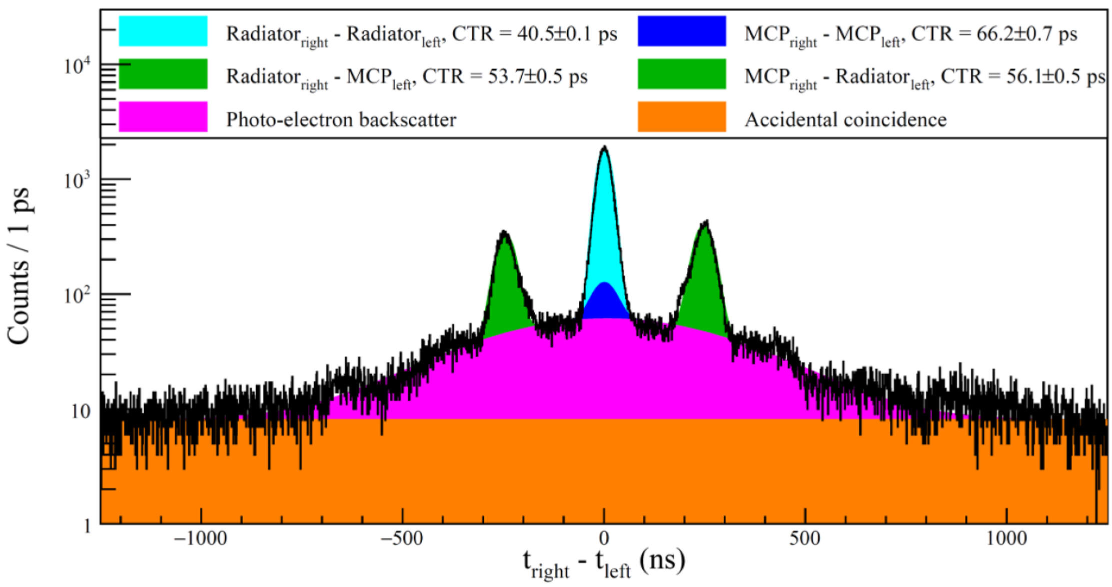

Figure 3. Timing histogram decomposed by the six event types. The main peak was decomposed into two Gaussians: Radiator–Radiator and MCP–MCP events. The CTR of the Radiator–Radiator and the MCP–MCP events were 40.5 and 66.2 ps FWHM, respectively. Note that the main peak in figure 1(b) is the sum of the light and dark blue peaks in this figure.

4. Discussion

The histogram of the time difference between the CRIs were decomposed into six types of interactions and the main peak was decomposed into the two types of interactions. In this section, more detail of the timing performance of the Radiator–Radiator and the MCP–MCP events were discussed.

The CTR of Radiator–Radiator events showed an improvement of 1.2 ps (from 41.7 ± 0.2 to 40.5 ± 0.1 ps FWHM) compared to the CTR where both the Radiator–Radiator and MCP–MCP events are mixed. Deterioration of the timing performance due to mixing can be calculated to be 9.9 ps ($\sqrt{41.7^2 - 40.5^2}$). Considering that both the Cherenkov radiator and the MCP consist of lead glass, removing the lead from the MCP but not from the Cherenkov radiator allows two advantages: (1) enhancement of timing performance and (2) elimination of the side peaks. From these points, a CRI with lead-free MCP should be targeted to achieve a CTR approaching 10 ps FWHM.

In this study, we do not apply the pulse area cut that could successfully improve the CTR from 41.9 ps to 30.1 ps FWHM, as in Ota *et al* (2019a). Thus, further scope exists for enhancing the timing performance by applying the pulse area cut, and we expect the CTR of the CRI with lead-free MCP to break the 30 ps barrier. However, such an event cut compromises the detection efficiency of the CRI. In actuality, only 3% of the largest pulse area events is used to obtain a CTR of 30.1 ps FWHM (Ota *et al* 2019a).

Regarding the total attenuation length, those of the LSO scintillator and the PbF_2 radiator are 11.5 and 9.5 mm, respectively (National Institute of Standards and Technology), whereas that of the lead glass radiator used in the CRI is 22.4 mm. In addition, lead glass is not transparent to UV photons, which are mostly emitted as Cherenkov photons; the radiator should be optimized in this context. The PbF_2 crystal is a potential candidate because it not only has higher stopping power than the LSO, but also shows higher transparency towards the UV region compared with lead glass (Anderson *et al* 1990). Thus, PbF_2-integrated MCP–PMT should be the next research objective. If two or three Cherenkov photons are detected on average

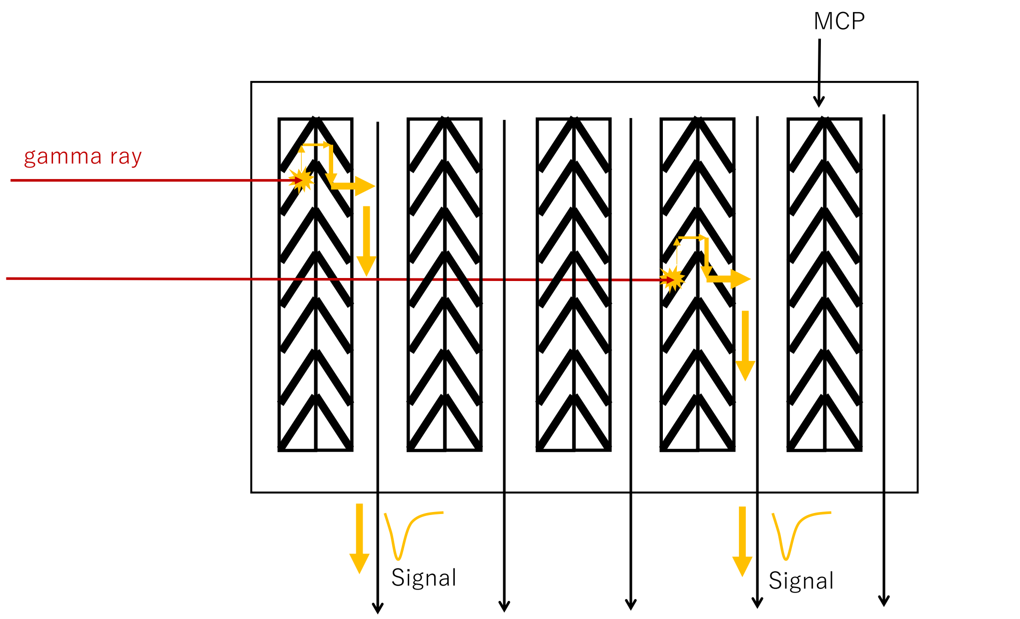

Figure 4. Concept of a radiation detector without any photocathodes. Elimination of the photocathode would result in an easy and robust construction and a potentially high radiation tolerance. By stacking several MCPs, the detection efficiency for gamma rays would be high. Additionally, high timing performance of CTR < 100 ps FWHM would be possible.

by the PbF_2-integrated MCP–PMT, we expect that the CTR can attain 30 ps FWHM without a reduction in the detection efficiency.

The detection efficiency of the MCP–MCP events was 6.2% of the Radiator–Radiator events. This means that single event detection efficiency of the MCP is 25% of the radiator. Despite of thinness of the MCP (0.24×2 mm) compared to the thickness of the radiator (3.2 mm), the detection efficiency of the MCP is relatively high. As discussed in (Brianza *et al* 2015) and (Barnyakov *et al* 2018), gamma rays sometimes interact with the MCP in the downstream section, and could not be adequately amplified due to the thinness of this amplification section. Therefore, the effective thickness of the MCP as a gamma-ray convertor may be as thin as 0.24 mm. The relatively high detection efficiency indicates that stacking several MCPs as illustrated in figure 4 could produce a gamma-ray detector with high detection efficiency. Notably, a photocathode is not required in the configuration shown in figure 4. Elimination of the photocathode would result in easy and robust construction of detectors with a potentially high radiation tolerance (Barnyakov *et al* 2018).

In addition, this detector can provide a high timing performance, i.e. a CTR of 66.2 ps FWHM (figure 3). Applying independent readout electronics would maintain the high timing performance, which would otherwise deteriorate in the multi-layered structure. The proposed detector could be a novel type of photodetector, and can be employed in applications where only the timing performance and the robustness of the detector are crucial.

5. Conclusions

We report an analytical method of deconvolution for removing MCP direct interactions from the histogram of time differences experimentally obtained using a pair of CRIs. Deconvolution provides an improvement in CTR from 41.7 to 40.5 ps FWHM. From this result, we find that the contribution of the MCP direct interactions to the CTR is of the order of 10 ps and that a new CRI based on lead-free MCP should be developed. The CTR of the MCP–MCP events is also evaluated and a CTR of 66.2 ps FWHM is obtained. In the case of the MCP direct interaction, a photocathode is not required. Therefore, this work not only points toward analytical tools to improve timing performance of CRI detectors, it also reveals the possibility of producing a high timing performance detector without a photocathode. Although the timing performance of a photocathode-free detector would be inferior to CRIs, elimination of the photocathode would make construction of the detector simple and robust.

Acknowledgment

Authors gratefully thank Dr. Eric Berg from the University of California, Davis for inspiring us the analysis methods.

ORCID iD

R Ota https://orcid.org/0000-0001-6345-1982

References

Anderson D F, Kobayashi M, Woody C L and Yoshimura Y 1990 Lead fluoride: an ultra-compact Cherenkov radiator for EM calorimetry *Nucl. Instrum. Methods* A **290** 385–9

Arino-Estrada G, Mitchell G S, Kim H, Du J, Kwon S I, Cirignano L J, Shah K S, Cherry S R *et al* 2019 First Cerenkov charge-induction (CCI) TlBr detector for TOF-PET and proton range verification *Phys. Med. Biol.* **64** 175001

Arino-Estrada G, Mitchell G S, Kwon S I, Du J, Kim H, Cirignano L J, Shah K S and Cherry S R 2018 Towards time-of-flight PET with a semiconductor detector *Phys. Med. Biol.* **63** 04LT01

Barnyakov A Y *et al* 2017 Micro-channel plates in ionization mode as a fast timing device for future hadron colliders *J. Inst.* **12** C08014

Barnyakov A Y *et al* 2018 Response of microchannel plates in ionization mode to single particles and electromagnetic showers *Nucl. Instrum. Methods* A **879** 6–12

Brianza L *et al* 2015 Response of microchannel plates to single particles and to electromagnetic showers *Nucl. Instrum. Methods* A **797** 216–21

Brun R and Rademakers F 1997 ROOT-an object oriented data analysis framework *Nucl. Instrum. Methods* A **389** 81–86

Brunner S E and Schaart D R 2017 BGO as a hybrid scintillator/Cherenkov radiator for cost-effective time-of-flight PET *Phys. Med. Biol.* **62** 4421

Cates J W, Gundacker S, Auffray E, Lecoq P, Levin C S *et al* 2018 Improved single photon time resolution for analog SiPMs with front end readout that reduce influence of electronic noise *Phys. Med. Biol.* **63** 185022

Cates J W and Levin C S 2019 Electronics method to advance the coincidence time resolution with bismuth germinate *Phys. Med. Biol.* **64** 175016

Conti M 2009 State of the art and challenges of time-of-flight PET *Phys. Med.* **25** 1–11

Gundacker S, Auffray E, Pauwels K, Lecoq P *et al* 2016 Measurement of intrinsic rise times for various L(Y)SO and LuAG scintillators with a general study of prompt photons to achieve 10 ps in TOF-PET *Phys. Med. Biol.* **61** 2802

Gundacker S, Turtos R M, Auffray E, Paganoni M and Lecoq P 2019 High-frequency SiPM readout advances measured coincidence time resolution limits in TOF-PET *Phys. Med. Biol.* **64** 055012

Hitomi K, Tada T, Onodera T, Shoji T, Kim S-Y, Xu Y, Ishii K *et al* 2013 Timing performance of TlBr detectors *IEEE Trans. Nucl. Sci.* **60** 2883–7

Hsu D F C, Ilan E, Peterson W T, Uribe J, Lubberink M and Levin C S 2017 Studies of a next-generation silicon-photomultiplier-based time-of-flight PET/CT system *J. Nucl. Med.* **58** 1511–18

Korpar S, Križan P, Pestotnik R and Stanovnik A 2008 Timing and cross-talk properties of BURLE multi-channel MCP-PMTs *Nucl. Instrum. Methods* A **595** 169–72

Kwon S I, Gola A, Ferri A, Piemonte C, Cherry S R *et al* 2016 Bismuth germanate coupled to near ultraviolet silicon photomultipliers for time-of-flight PET *Phys. Med. Biol.* **61** L38

Kwon S I, Roncali E, Gola A, Paternoster G, Piemonte C and Cherry S R 2019 Dual-ended readout of bismuth germanate to improve timing resolution in time-of-flight PET *Phys. Med. Biol.* **64** 105007

Lecoq P 2017 Pushing the limits in time-of-flight PET imaging *IEEE Trans. Rad. Plasma Med. Sci.* **1** 473–85

Lecoq P, Auffray E, Brunner S, Hillemanns H, Jarron P, Knapitsch A, Meyer T, Powolny F *et al* 2010 Factors influencing time resolution of scintillators and ways to improve them *IEEE Trans. Nucl. Sci.* **57** 2411–16

Lecoq P, Korzhik M, Vasiliev A *et al* 2014 Can transient phenomena help improving time resolution in scintillators? *IEEE Trans. Nucl. Sci.* **61** 229–34

Li V A *et al* 2018 Studies of MCP-PMTs in the miniTimeCube neutrino detector *AIP Adv.* **8** 095003

Moszynski M, Gresset C, Vacher J, Odru R *et al* 1981 Timing properties of BGO scintillator *Nucl. Instrum. Methods* A **188** 403–9

National Institute of Standards and Technology 2019 (https://physics.nist.gov/PhysRefData/Xcom/html/xcom1.html Accessed: 2 March 2020)

Ota R, Nakajima K, Hasegawa T, Ogawa I, Tamagawa Y *et al* 2019b Timing-performance evaluation of Cherenkov-based radiation detectors *Nucl. Instrum. Methods* A **923** 1–4

Ota R, Nakajima K, Ogawa I, Tamagawa Y, Shimoi H, Suyama M and Hasegawa T 2019a Coincidence time resolution of 30 ps FWHM using a pair of Cherenkov-radiator-integrated MCP-PMTs *Phys. Med. Biol.* **64** 07LT01

Ota R, Yamada R, Moriya T, Hasegawa T *et al* 2018 Cherenkov radiation-based three-dimensional position-sensitive PET detector: a Monte Carlo study *Med. Phys.* **45** 1999–2008

Rausch I, Ruiz A, Valverde-Pascual I, Cal-González J, Beyer T, Carrio I *et al* 2019 Performance evaluation of the Vereos PET/CT system according to the NEMA NU2-2012 standard *J. Nucl. Med.* **60** 561–7

Sluis J, de Jong J, Schaar J, Noordzij W, van Snick P, Dierckx R, Borra R, Willemsen A, Boellaard R *et al* 2019 Performance characteristics of the digital biograph vision PET/CT system *J. Nucl. Med.* **60** 1031–6

Vandenberghe S, Mikhaylova E, D'Hoe E, Mollet P, Karp J S *et al* 2016 Recent developments in time-of-flight PET *EJNMMI Phys.* **3** 3